



RESEARCH ARTICLE

Quantitative proteomics of hamster lung tissues infected with SARS-CoV-2 reveal host factors having implication in the disease pathogenesis and severity

Voddu Suresh^{1,2} | Varshasnata Mohanty¹ | Kiran Avula^{1,2} | Arup Ghosh^{1,3} | Bharati Singh^{1,3} | Rajendra Kumar Reddy¹ | Deepti Parida^{1,2} | Amol Ratnakar Suryawanshi¹ | Sunil Kumar Raghav¹ | Soma Chattopadhyay¹ | Punit Prasad¹ | Rajeeb Kumar Swain¹ | Rupesh Dash¹ | Ajay Parida¹ | Gulam Hussain Syed¹  | Shantibhusan Senapati¹ 

¹Institute of Life Sciences, Bhubaneswar, India

²Regional Centre for Biotechnology, Faridabad, India

³Kalinga Institute of Industrial Technology, Bhubaneswar, India

Correspondence

Gulam Hussain Syed and Shantibhusan Senapati, Institute of Life Sciences, Nalco Square, Bhubaneswar 751023, Odisha, India.

Email: gulamsyed@ils.res.in (G. H. S.); senapati@ils.res.in (S. S.)

Funding information

DBT-BIRAC, India, Grant/Award Number: BT/CS0004/CS/02/20

Abstract

Syrian golden hamsters (*Mesocricetus auratus*) infected by severe acute respiratory syndrome coronavirus 2 (SARS-CoV-2) manifests lung pathology. In this study, efforts were made to check the infectivity of a local SARS-CoV-2 isolate in a self-limiting and non-lethal hamster model and evaluate the differential expression of lung proteins during acute infection and convalescence. The findings of this study confirm the infectivity of this isolate in vivo. Analysis of clinical parameters and tissue samples show the pathophysiological manifestation of SARS-CoV-2 infection similar to that reported earlier in COVID-19 patients and hamsters infected with other isolates. However, diffuse alveolar damage (DAD), a common histopathological feature of human COVID-19 was only occasionally noticed. The lung-associated pathological changes were very prominent on the 4th day post-infection (dpi), mostly resolved by 14 dpi. Here, we carried out the quantitative proteomic analysis of the lung tissues from SARS-CoV-2-infected hamsters on day 4 and day 14 post-infection. This resulted in the identification of 1585 proteins of which 68 proteins were significantly altered between both the infected groups. Pathway analysis revealed complement and coagulation cascade, platelet activation, ferroptosis, and focal adhesion as the top enriched pathways. In addition, we also identified altered expression of two pulmonary surfactant-associated proteins (Sftpd and Sftpb), known for their protective role in lung function. Together, these findings will aid in understanding the mechanism(s) involved in SARS-CoV-2 pathogenesis and progression of the disease.

Abbreviations: ABSL3, animal biosafety level 3; AERD, aspirin exacerbated respiratory disease; ARDS, acute respiratory distress syndrome; BAL, bronchoalveolar lavage; BCA, biconchonic acid assay; CF, cystic fibrosis; DAD, diffuse alveolar damage; DAPI, 4', 6-diamidino-2-phenylindole; DTT, dithiothreitol; HPLC, high performance liquid chromatography; IAA, iodoacetamide; PANTHER, protein analysis through evolutionary relationships; PBST, phosphate-buffered saline with tween detergent; PCA, principal component analysis; TEABC, triethylammonium bicarbonate.

Voddu Suresh, Varshasnata Mohanty and Kiran Avula are contributed equally.

KEYWORDS

COVID-19, differentially expressed proteins, lung proteome, mass spectrometry, Orbitrap, pulmonary surfactant, SARS-CoV-2

1 | INTRODUCTION

The recent outbreak of severe acute respiratory syndrome coronavirus 2 (SARS-CoV-2) has emerged as a global public health crisis affecting millions of people worldwide. SARS-CoV-2, the causative agent of the coronavirus disease 2019 (COVID-19), primarily infects the respiratory tract resulting in respiratory failure consistent with the acute respiratory distress syndrome (ARDS). The aggressive inflammatory response associated with infection leads to tissue damage and fatal lung injury. The death of the virus affected epithelial cells and endothelial cells, and activation of resident dendritic cells, monocytes, and macrophages result in the dysregulated inflammatory response. This triggers further activation and recruitment of immune cells leading to tissue damage and exacerbation of respiratory distress and disease severity. However, the levels of circulating cytokines in COVID-19 patients are found to be lower in comparison to patients experiencing ARDS due to other reasons¹ and post-mortem investigation of COVID-19 patients revealed severe vascular injury including alveolar microthrombi.² Virus-induced coagulopathy has also been implicated to trigger COVID-19 associated pneumonia and ARDS.³ Currently, our understanding of COVID-19 associated lung injury is limited and requires further studies to elucidate the intricate and specific mechanisms.

Severe clinical manifestations involving multi-organ failure have resulted in high morbidity and mortality, thus demanding immediate therapeutic measures and disease management. In this regard, a better understanding of viral and host factors involved in this disease's pathogenesis has paramount significance. After identifying the SARS-CoV-2 virus, multiple genomic and proteomics-based approaches have been adapted to understand the host response to this viral infection. In the recent past, different studies have been conducted using proteomics technology to understand the virus-host protein interactome, changes in host protein expression upon virus infection, and for diagnosis of SARS-CoV-2 infection. Most of these studies have been carried out with patients' liquid specimens like serum, plasma, sputum, and bronchoalveolar lavage.⁴⁻⁸ Clinical manifestations of COVID-19 are primarily related to the lung; hence clinical proteomics of infected lung tissues are essential to understand and combat this disease. The information obtained from such studies will provide the rationale for designing novel diagnostic and therapeutic interventions. Using lung tissues obtained from a small number of deceased COVID-19

patients, an earlier study has identified differentially expressed proteins in biological processes like blood coagulation, metabolism, immune response, angiogenesis and cell microenvironment regulation.⁹ Another group has extracted proteins from Formalin-Fixed Paraffin-Embedded (FFPE) lung tissues of COVID-19 deceased patients and identified high expression of proteins associated with SARS-CoV-2 entry (cathepsins B and L) and inflammatory response modulator (S100A8/A9).¹⁰ In a recent study, proteomic analysis of autopsy samples of nineteen COVID-19 patients showed the elevation of cathepsin L1, rather than ACE2 in infected lung tissues and highlighted the dysregulation of biological processes like angiogenesis, coagulation, and fibrosis in different organs including lungs. Most of these studies report the upregulation of proteins predominantly implicated in the hyperinflammatory state, repair state, and lung fibrosis.^{10,11} However, so far no experimental controlled lung proteomics study is available to characterize the molecular mechanisms underlying COVID-19 pathogenesis at different stages of the disease progression. Preclinical animal models that recapitulate multiple sequential events associated with human diseases are precious tools to understand the mechanistic aspects of human disease progression. In human patients, the COVID-19 associated lung pathology is a major clinical concern.^{12,13}

At present, no animal model recapitulates all aspects of COVID-19 in humans.^{14,15} Among different available animal models, so far hamsters have been widely utilized in SARS-CoV-2 infection studies. Hamster model of COVID-19 mimics a mild pattern of human disease with full recovery.¹⁶⁻²⁰ Although SARS-CoV-2 infection of hamsters induces lung pathologies like pulmonary edema, consolidation, and interstitial pneumonia, but failed to develop diffuse alveolar disease, a prominent clinical feature noticed in COVID-19 patients experiencing severe disease.^{18,21} Further characterization of this model is essential for the development of effective therapeutics and vaccines against this virus. An in-depth understanding of host response to SARS-CoV-2 infection in hamsters will elucidate this model's similarity or dissimilarity with human patients. Although efforts to identify differentially expressed proteins in diverse body fluids of COVID-19 patients were made, there is a dearth of evidence related to differentially expressed proteins in human lung tissues at acute and convalescent stages of SARS-CoV-2 infection. Fresh lung tissues of COVID-19 patients during infection or recovery are ethically impossible to obtain. Hence, so far, data obtained

from tissues of deceased COVID-19 patients are only available. In this regard, tissues obtained from animals infected with SARS-CoV-2 at different days post-infection will prove beneficial. In this study, efforts have been made to quantitatively compare the lung proteome in SARS-CoV-2-infected hamsters at various days post-infection. The differentially expressed proteins identified in this study will provide information on various host proteins that might have a significant role in the pathogenesis of SARS-CoV-2 infection or disease manifestation. Some of the differentially expressed proteins identified in this study can also be validated in easily accessible patient samples such as body fluids as potential biomarkers for predicting the disease course.

2 | MATERIALS AND METHODS

2.1 | Animal ethics

In this study, attempts were made to evaluate the infectivity of one of the local isolates of SARS-CoV-2, IND-ILS01/2020 (GenBank accession ID-MW559533.2) in the Syrian Golden Hamster model. All the experiments were performed with prior approval of the Institutional Biosafety Committee (IBSC) and Institutional Animal Ethical Committee (IAEC). The study was carried out adhering to the guidelines of the Committee for the Purpose of Control and Supervision of Experiments on Animals (CPCSEA), Govt. of India.

2.2 | Animal studies

For this study, eleven hamsters of the age group 6-7 months were acclimatized at the ILS ABSL3 facility for 4-6 days prior to the experiments. As shown in the schematic (Figure 1A), on day zero, six animals were infected intranasally with SARS-CoV-2 (10^5 TCID₅₀)¹⁸ and five animals were mock-infected (only PBS) under intraperitoneal ketamine (200 mg/kg) and xylazine (10 mg/kg) anesthesia. The SARS-CoV-2 virus used in this study was isolated from a clinically confirmed local COVID-19 patient (IND-ILS01/2020; GenBank accession ID-MW559533.2). Virus stock from the 10th passage was titrated by plaque and TCID₅₀ (Median Tissue Culture Infectious Dose) assays and used for this animal challenge study. Out of the six infected animals, three animals were sacrificed on 4 dpi (day post-infection), and the other three were sacrificed on 14 dpi. Out of the five mock-infected animals, three were sacrificed on 4 dpi, and the other two were sacrificed on 14 dpi. Throughout the experiment, all the animals were monitored daily, and body weights were recorded on alternate days. On the day of sacrifice, tissues

from all the vital organs and other organs like the pancreas, spleen, and gastrointestinal tracts were harvested, preserved, and further processed for histopathological analysis and viral load estimation. All the groups had two male and one female animal, except the 14 dpi mock-infected group, which had one male and one female animal in it.

2.3 | Sample collection, storage, and processing

Tissues harvested from different organs, including lungs, were divided into three parts. One part was stored in buffered formalin and further processed for histopathological analysis. The second part was immediately put into TRIzol RNA isolation buffer, and the third part was snap-frozen and stored at -80°C until further use. Formalin-fixed tissues were further processed and sectioned for Hematoxylin and Eosin (H&E), Immunohistochemistry (IHC), and Immunofluorescence analysis (IF) as reported earlier.²²

2.4 | Hematoxylin and Eosin (H&E) staining and lung pathology scoring

Tissues from multiple lobes of all the animals were processed and stained with H&E staining. Stained lung sections were assigned with different numbers and evaluated in a blinded fashion. Lung pathology scoring was performed similarly as reported by Li et al²³ The scoring was performed in a blinded fashion and cross-validated by two experienced evaluators. Briefly, the sections were scored for three major pulmonary pathological features associated with SARS-CoV-2 infection (bronchiolitis, alveolitis, and vasculitis/endotheliitis) (Supplementary Figure S1). Each feature was scored on a scale of 0-4 and the total score was obtained by adding values for each feature. The total score ranged between 0 and 12.

2.5 | Immunohistochemistry

Collected tissues were processed and sectioned as reported previously.^{22,24} Sections were deparaffinized, rehydrated, and subjected to antigen retrieval (Vector Laboratories) treatment for 20 minutes followed by blocking the endogenous peroxidase with 3% hydrogen peroxide in methanol for 20 minutes. Horse serum (Vector Laboratories) was used for blocking the sections for 30 minutes at room temperature and incubated with Ki-67 antibody (#VP-RM04; Vector Laboratories, 1:100) or rabbit polyclonal anti-human Sftpd antibody (1:500) antibody overnight at 4°C .²⁵ Sections were washed twice

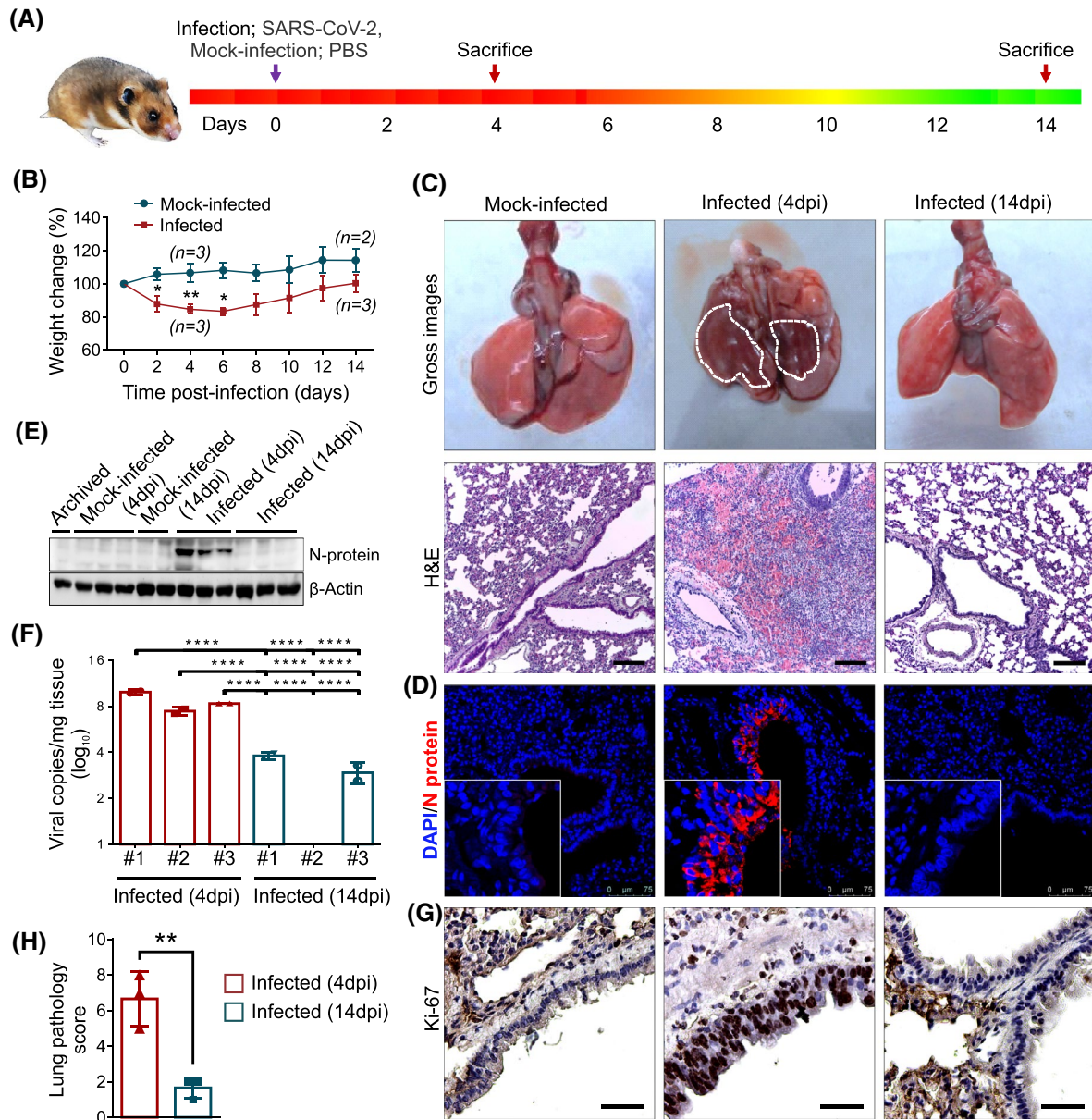


FIGURE 1 Syrian Golden Hamster model of SARS-CoV-2 infection by a local SARS-CoV-2 isolate. A, Study design to evaluate the infectivity of local-isolate in Syrian Golden Hamster infection model. B, Graph showing percent body weight change in hamsters after mock-infection or SARS-CoV-2 infection. C, Digital images of lungs harvested from mock-infected or infected animals. At 4 dpi, infected lungs have massive congestions visible from the surface (highlighted with white border). No gross changes were noticed in mock-infected (4 dpi) and infected (14 dpi) lungs. Images showing H&E stained lung tissues harvested from mock-infected or infected (4 or 14 dpi) hamsters (scale bar = 200 μ m). D, Immunofluorescence images of mock-infected or infected lung tissue sections showing presence of Nucleocapsid protein (N) in bronchial and alveolar epithelial cells. E, Immunoblot analysis showing the Nucleocapsid protein expression in the lungs previously archived lysate (normal), mock-infected (4 dpi), infected 4 dpi or 14 dpi lung tissues. F, Graph showing the viral RNA quantification by RT-qPCR in hamster lung tissues. G, Immunohistochemistry staining with Ki67 showing cell proliferation of bronchial and alveolar cells (scale bar = 50 μ m). H, Graph showing pathology score of the lung tissues after the infection (4 and 14 dpi)

with 1 \times PBS and treated with biotinylated anti-rabbit/mouse IgG secondary antibody (Vector Laboratories) for 45 minutes, followed by ABC reagent for 30 minutes. Diaminobenzidine (Vector Laboratories) was used as a substrate to develop the stain. Hematoxylin was used as

a counterstain followed by dehydration with alcohol, clearing with xylene, and mounting with permanent mounting media (Vector Laboratories). Stained sections were observed under the microscope (Leica DM500), and images were taken at different magnifications.

2.6 | Immunofluorescence

Sections were deparaffinized, rehydrated, and subjected to antigen retrieval treatment and serum blocking as reported earlier.²² Sections were incubated with SARS-CoV-2 N protein (Nucleocapsid) (#11-2003; Abgenex, 1:200) or SOD2/Mn-SOD (#NB100-1992; Novus biologicals, 1:100) in a humidified chamber overnight at 4°C. Sections were washed twice with PBST for 5 minutes each and incubated with anti-Rabbit Alexa Fluor 594 (#A-11037; Life technologies, 1:500) or anti-Mouse Alexa Fluor 594 (#A-11005; Life technologies, 1:500) for 45 minutes under dark conditions at room temperature. Sections were washed with PBST twice and mounted with ProLong Gold Antifade reagent with DAPI (#P36935; Invitrogen) and visualized using Leica TCS SP8STED confocal microscope.

2.7 | Western blot analysis

For Western blot analysis, cells were re-suspended in Radioimmunoprecipitation assay (RIPA) buffer (20 mM Tris-HCl, pH 7.5, 150 mM NaCl, 50 mM NaF, 1 mM Sodium orthovanadate (Na_3VO_4), 0.1% SDS, and 0.5% TritonX-100) containing the protease inhibitor cocktail (Thermo Scientific). The whole-cell lysates (WCL) were subjected to SDS-PAGE and transferred to nitrocellulose membrane (Thermo Scientific), followed by blocking and immunoblotting with antibodies specific for SARS-CoV-2 Nucleocapsid protein (#11-2003, Abgenex) or β -actin (#4970, CST).²⁶

2.8 | qRT-PCR

RNA isolation was carried out from hamster tissue samples using TRizol reagent (#10296010, Invitrogen). The isolated RNA was subjected to qRT-PCR for determining the viral load. We performed one-step multiplex real-time PCR using TaqPath 1-Step Multiplex Master Mix (#A28526, Thermo Fisher Scientific), targeting SARS-CoV-2 gene with primer and probe set specific for nucleocapsid (N). The standard curve for absolute quantification of viral genome copies was generated using log-fold dilutions of plasmid harboring the SARS-CoV-2 nucleocapsid gene.²⁷

2.9 | Sample preparation for proteomics analysis

The lung tissue samples of SARS-CoV-2-infected on 4 and 14 dpi along with mock-infected (4 dpi) were processed and homogenized using liquid nitrogen and lysed in lysis buffer containing 4% sodium dodecyl sulfate (SDS) and 50 mM

triethylammonium bicarbonate (TEABC). The samples were subjected to sonication three times for 10 seconds storing on ice to prevent overheating between the sonication and were followed by heating at 90°C for 5 minutes. The lysates were then incubated at room temperature for cooling and centrifuged at 12 000 rpm for 10 minutes. The protein concentration present in the supernatant was determined using a bicinchoninic acid assay (BCA) kit (Thermo Scientific Pierce) and an equal amount of protein from each group was pooled for further analysis. LC-MS/MS approach was used using isotopomer labels, “tandem mass tags” (TMTs), to determine the relative quantification of proteins.²⁸

2.10 | In-solution digestion and TMT labeling

Protein lysate of 300 μg from pooled samples of each group was reduced by incubating in 10mM Dithiothreitol (DTT) at 60°C for 20 minutes. Alkylation was carried out in the dark with 20 mM iodoacetamide (IAA) at room temperature for 10 minutes. The lysate was further subjected to acetone precipitation, and the pellet was dissolved in 50 mM TEABC. Digestion was carried out at 37°C for 16 hours using trypsin (Sciex, #4326682) at a final concentration of 1:20 (w/w). The reaction was acidified using 0.1% formic acid, and the peptides were lyophilized and stored at -80°C until further use.

2.11 | LC-MS/MS acquisition

The digested peptides were fractionated into six fractions using StageTip fractionation. Fractionated peptides (6 fractions in triplicate, total of 18 runs) were analyzed on Orbitrap Fusion Tribrid mass spectrometer (Thermo Fisher Scientific, Bremen, Germany) interfaced with EASY-nLC 1000 nanoflow liquid chromatography system (Thermo Scientific, Odense, Southern Denmark). Each fraction was reconstituted in solvent A (0.1% formic acid) and loaded onto trap column (75 $\mu\text{m} \times 2 \text{ cm}$) Thermo Scientific Acclaim PepMap 100 C18 (#164535; Thermo Scientific) (3 μm particle size, pore size 100 \AA) at a flow rate of 5 $\mu\text{l}/\text{min}$ with solvent A (0.1% formic acid in water).

The peptides were resolved on an analytical column (EASY-Spray C18 Reversed Phase HPLC Column, 2 μm , 75 $\mu\text{m} \times 500 \text{ mm}$; Thermo Scientific) using a linear gradient of 7%-30% solvent B (0.1% formic acid in 95% acetonitrile) over 100 minutes at a flow rate of 300 nL/min. Data-dependent Mass Spectrometry acquisition was carried out at *top speed* mode with full scans (350-1500 m/z) acquired using an Orbitrap mass analyzer at a mass resolution of 120 000 at 200 m/z . For MS/MS, top intense precursor ions from a 3-second duty cycle were selected and subjected to higher-energy collision dissociation (HCD) with 35% normalized collision energy. The

fragment ions were detected at a mass resolution of 30 000 at m/z of 200. Dynamic exclusion was set for 30 seconds. Lock-mass from ambient air (m/z 445.1200025) was enabled for internal calibration as described previously.²⁹

2.12 | Bioinformatics and statistical analysis

The Proteome Discoverer 2.3 (Thermo Scientific, Bremen, Germany) was used to carry out protein identification and quantitation. All raw files were searched against a *Mesocricetus auratus* (Syrian Golden hamster) protein database in Universal Proteins Resource Knowledgebase (UniProt) (32,336 entries) supplemented with common contaminants (116 entries) using SequestHT as a search algorithm. The search parameters included trypsin as the proteolytic enzyme with a maximum allowed missed cleavages to two. Oxidation of methionine and acetylation of protein N-terminus were set as dynamic modifications. In contrast, static modifications included cysteine carbamidomethylation and TMT modification at the N-terminus of the peptide and lysine residue. Precursor mass tolerance was set to 10 ppm, and fragment mass tolerance was set to 0.05 Da. Peptide Spectrum Matches were identified at 1% False Discovery rate. The differential expression ratios between the groups were calculated. Proteins with differential expression ratios ≥ 1.5 (upregulated) or ≤ 0.67 (downregulated) were considered as differentially expressed. The significance of differences between groups was calculated using *Student's t test* (two-tailed), and a P -value $\leq .05$ was considered statistically significant. All the differentially expressed proteins across the two groups (Infected 4 dpi and infected 14 dpi) were compared using a Venn diagram (Venny 2.1, <https://www.bioinfogp.cnb.csic.es/tools/venny/>) and further analyzed with PANTHER classification system, version 16.0 (<http://www.pantherdb.org>). Gene Ontology (GO) and pathway analysis using Kyoto Encyclopedia of Genes and Genomes (KEGG) were performed using the Enrichr online tool (<http://www.ampharm.mssm.edu/Enrichr/>).³⁰

Principal component analysis was performed using sample-wise scaled unfiltered normalized protein abundance data using PCAtools. Heatmaps were generated using protein-wise scaled and filtered protein abundance (1.5 and 1.3 up- or down-regulation; P -value $\leq .05$ in any comparison) and k -means clustering ($k = 3$).

3 | RESULTS

3.1 | Clinical features, viral load, and histopathological changes in lungs

To investigate the pathogenicity of SARS-CoV-2, Syrian hamsters were infected with the virus, and harvested tissue

samples were collected at two different time points (4 & 14 dpi) for viral load and pathological analysis (Figure 1A). Corroborating earlier reports, a significant weight loss was noticed in all the infected animals at 4 dpi. On 4 dpi, all the animals lost around 15% of their initial body weight (Figure 1B). After 6 dpi, the infected animals started regaining their body weight. During the course of the experiments, no mortality was found in both infected and mock-infected animals. At the time of organ isolation, congestion of lungs was grossly visible only in infected animals at 4 dpi (Figure 1C). Further histopathological analysis of the 4 dpi SARS-CoV-2-infected tissue samples showed the presence of severe pathological lesions in the lungs (Figure 1C and Supplementary Figure S1A-G). Multifocal necrosis and the desquamation of bronchial epithelial cells and infiltration of inflammatory cells were present in the SARS-CoV-2-infected lung tissues (Figure 1C). Around 50% lung area was affected in all the infected animals, and the lesions were patchy throughout the lungs. Necrosuppurative bronchitis and interstitial pneumonia were evident in all the infected animals at 4 dpi (Supplementary Figure S1D,E). Different areas of the infected lung tissues showed consolidation of lungs and hemorrhage (Supplementary Figure S1C). These hamsters exhibited severe interstitial pneumonia, as evidenced by the thickening of the alveolar wall, altered alveolar structure, and immune cells' infiltration (Supplementary Figure S1D). At 4 dpi, infected lungs have occasional features of diffuse alveolar damage (DAD) including necrosis of alveolar epithelial cells, presence of intra-alveolar immune cells, cellular debris, and protein exudates (Supplementary Figure S1F). However, hyaline membrane formation was very rarely noticed, which indicates a less severe form of DAD.³¹ Endothelium near the damaged areas was reactive, as evidenced by mononuclear cells' adhesion to the endothelium (Supplementary Figure S1A). In certain instances, the immune cells have invaded the vessel wall and caused endotheliitis (Supplementary Figure S1B). In one of the infected animals (4 dpi), visceral pleural invasion of immune cells was also noticed (Supplementary Figure S1G). However, no noticeable histopathological changes were observed in mock-infected hamster lung at any time point. After 14 dpi, hamsters infected with SARS-CoV-2 exhibited only mild inflammatory infiltration and tissue damage suggestive of the resolution of disease manifestation (Figure 1C). Histopathological evaluation of tracheal tissues from all the animals also showed severe tracheal epithelial and endothelial damage in 4 dpi-infected tissues compared to 14 dpi-infected or mock-infected tissues (Supplementary Figure S2). The significantly higher lung pathology score at 4 dpi-infected tissues than 14 dpi corroborates the earlier reports and indicates the self-limiting nature of this disease in the hamsters (Figure 1H).

Immunofluorescence (IF) staining of lung tissue sections with SARS-CoV-2 nucleocapsid (N) protein showed the viral antigen-positive bronchial and alveolar epithelial cells at 4 dpi, which were not detected at 14 dpi tissues (Figure 1D). Immunoblot analysis of the lung tissue protein lysates also corroborated the IF findings (Figure 1E). The viral genome copy number estimation showed the presence of viral genome in both 4 dpi and 14 dpi-infected lung tissues; however, the copy number was significantly low in 14 dpi tissues compared to 4 dpi tissues (Figure 1F). Immunohistochemical staining for Ki67, a marker of cell proliferation, showed marked cellular proliferation (hyperplasia) of bronchial and alveolar cells at 4 dpi (Figure 1G). This finding corroborates with the earlier report.²⁰

3.2 | Quantitative proteomics analysis

3.2.1 | Molecular alterations in pulmonary pathology induced by SARS-CoV-2 infection

Analysis of all the animals' body weights, lung pathology, and status of viral protein in lung tissues clearly demonstrated normal animal health in both the 4 dpi and 14 dpi mock-infected animals. At the same time, lung tissues from the 4 dpi and 14 dpi-infected hamsters manifested features of acute and convalescent stages of the infection, respectively. One of the major objectives of the current study was to compare the lung proteome of SARS-CoV-2-infected hamster lung tissues at acute and convalescent stages of the infection. Hence, we employed a quantitative proteomics approach to identify the proteomic alterations in hamster lung tissue induced by SARS-CoV-2 at different time points (4 dpi and 14 dpi) compared with only 4 dpi mock-infected control tissues (as a representative of mock-infected groups). The quantitative proteomics data were analyzed using high-resolution LC-MS/MS in triplicates where the raw files were searched using Proteome Discoverer 2.3. The search resulted in the identification of 1585 proteins expressed across all the samples. Of these, 50 and 18 proteins were differentially expressed (cut off 1.5-fold, $P \leq .05$) at 4 dpi and 14 dpi, respectively. The 50 differentially expressed proteins in 4 dpi included 33 upregulated and 17 downregulated proteins whereas 18 differentially expressed proteins in 14 dpi included nine upregulated and nine downregulated proteins. A complete list of the proteins identified is provided in Supplementary Table S1. All the differentially expressed proteins were further represented as a heat map using hierarchical clustering analysis comparing mock-infected with the infected samples (Figure 2A). Interestingly, the principal component analysis (PCA) demonstrated distinct protein expression patterns among the mock-infected 4 dpi and

14 dpi-infected samples, depicting variation among them (Figure 2B). In PC1, we observed distinct clusters of data representing the 14 dpi and 4 dpi lung tissue samples, and separate clusters representing the mock-infected (4 dpi) and 14 dpi samples in PC2. Technical triplicate samples of the same groups are clustered together.

We compared all the identified proteins across the two groups (Infected 4 dpi and infected 14 dpi) to identify the number of common and differentially expressed proteins. This comparison was carried out using a Venn diagram (Venny 2.1, <https://www.bioinfogp.cnbc.csic.es/tools/venny/>). Upon comparison, we identified 41 proteins exclusive to 4 dpi tissue samples and nine exclusive to 14 dpi tissue samples when compared with mock-infected (4 dpi) tissue samples, while nine proteins were shared between the groups (Supplementary Figure S3). Of the total identified proteins, 50 proteins were differentially expressed (33 upregulated and 17 downregulated; $P \leq .05$) in 4 dpi-infected groups. Among these proteins, majority were involved in the blood coagulation, integrin signaling pathway, alternative complement activation signaling pathway, and plasminogen activating cascade (PANTHER classification system, version 16.0).³² Similarly, 18 proteins were differentially expressed (nine upregulated and nine downregulated; $P \leq .05$) in the infected 14 dpi group. This included proteins belonging to the plasminogen activating cascade and PI3K-Akt signaling pathway. The differentially expressed proteins are graphically represented as a heat map and volcano plots representing distinct proteomic patterns between the two groups compared to mock-infected (Supplementary Figure S4A-C). We also evaluated the altered protein expression during the acute and convalescent stages of infection (14 dpi vs 4 dpi) (Supplementary Figure S4D).

We further compared the differentially expressed proteins of statistical significance across the SAR-CoV2-infected (4 dpi and 14 dpi) and mock-infected (4 dpi) groups. A comparison of the downregulated proteins and upregulated proteins from both groups did not result in any common protein. However, among the 33 proteins upregulated in the 4 dpi tissue samples, three proteins such as superoxide dismutase (Sod2), myosin-2 (Myh2), and calgranulin-B (S100a9) were downregulated in the 14 dpi tissue samples. These proteins are known to regulate various cellular processes such as antioxidant defense, cellular localization, cell adhesion, and cellular migration. Similarly, among the 33 proteins upregulated in the 4 dpi lung tissue, four proteins, including Fibrinogen beta chain (Fgb), Ferritin (Fth1), Calpactin I (S100a10), Thymosin (Tmsb4x) were found to be upregulated in a 14 dpi sample. These proteins were involved in the regulation of biological processes and exhibit catalytic activity. On further comparison of downregulated proteins identified across

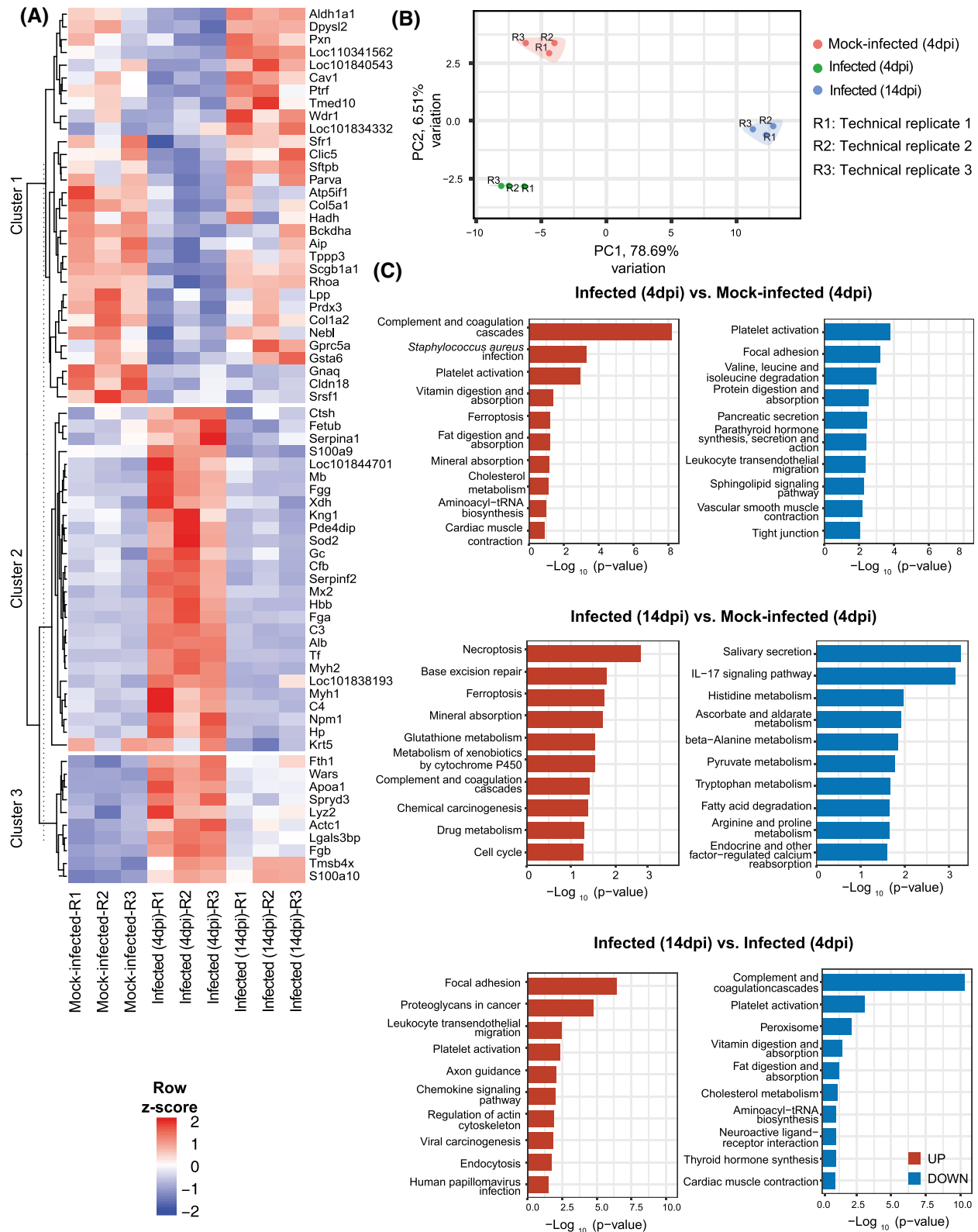


FIGURE 2 Lung tissue proteome of hamsters infected with SARS-CoV-2 at different time points. A, Heatmap of the differential expressed proteins ($P \leq .05$; fold change cut off of 1.5) were plotted sample wise suggesting the proteomic alterations across the infected samples (4 and 14 dpi) compared to mock-infected (4 dpi). B, Principal Component Analysis (PCA) was performed and plotted using PCAtools with technical replicates marked by R1, R2, and R3. The PCA plot represents the variance explained by the principal components (denoted by PC) indicating a clear separation of the samples among the three groups, ie, mock-infected (4 dpi), infected (4 dpi), and infected (14 dpi). C, Pathway analysis was performed using Enrichr online tool using the KEGG database. The enrichment analysis was performed for upregulated and downregulated differentially expressed proteins for all the three groups infected (4 dpi) versus mock-infected (4 dpi); Infected (14 dpi) versus mock-infected (4 dpi); and infected (14 dpi) versus infected (4 dpi). The horizontal axis represents the enrichment score $-\log_{10}(P\text{-value})$ of the pathway and the vertical axis represents the pathway category. The red color represents upregulated proteins and the blue bar represents downregulated proteins

both 4 dpi- and 14 dpi-infected tissues, two proteins were common in both groups, the serine/arginine-rich splicing factor 1 (Srsf1) and Guanine nucleotide-binding protein G (q) subunit alpha (Gnaq).

3.2.2 | Functional characteristic of significantly altered proteins

To systematically investigate the molecular differences in the hamster lung owing to SARS-CoV-2 infection, we carried out a Gene Ontology (GO) analysis of the differentially expressed proteins. The biological process such as “platelet degranulation,” “regulated exocytosis,” and “fibrinolysis” were enriched mainly in the proteins upregulated in infected (4 dpi) lung tissues, whereas “wound healing,” “collagen fibril organization,” and “actin cytoskeleton reorganization” were enriched in downregulated proteins (Supplementary Table S2). The proteins associated with these pathways include fibrinogens (Fga, Fgb, and Fgg); complement factors (C4a, C3); alpha-2-antiplasmin (Serpinf2); Alpha-1-B Glycoprotein (A1bg), Apolipoprotein A1 (Apoa1), and Alpha-1-acid glycoprotein 1 (Orm1). Notably, the terms such as “regulation of substrate adhesion-dependent cell spreading” and “endothelial cell migration” were mostly observed in upregulated and downregulated proteins in 14 dpi (Supplementary Table S3).

3.2.3 | Pathway analysis

KEGG pathway analyses of the differentially expressed proteins in lung tissue at 4 dpi compared to mock-infected (4 dpi) tissue revealed that SARS-CoV-2-triggered the activation of complement and coagulation cascade and ferroptosis. The analysis also resulted in the identification of other aberrant pathways such as platelet activation, focal adhesion, and tight junction. Interestingly, we also observed an aberrant expression of proteins associated with necroptosis, cholesterol metabolism, ferroptosis, and interleukin-17 signaling pathway in the 14 dpi tissue samples suggestive of the underlying mechanisms that lead to tissue damage and lung injury during SARS-CoV-2 infection (Figure 2C).

3.3 | Secretory proteins

To investigate the amount of secretory proteins among the pool of differentially expressed proteins in the infected tissue samples, we compared our data with the proteins annotated as “secretory proteins (2640 proteins),” “Secreted in the blood (729 proteins),” “Lung enriched (13 proteins),” “Lung proteome (19 649 proteins),” and “Group enriched

(61 proteins expressed in the lung)” (Supplementary Figure S4E). We found four proteins, Advanced Glycosylation End-Product-Specific Receptor (Ager), secretoglobin family 1A member 1 (Scgb1a1), Surfactant associated protein B (Sftpb), and Surfactant associated protein D (Sftpd) identified in the current study were specific to lung proteome.

3.4 | Validation of selected proteins’ expression status

To validate the hamster lung proteome data identified in this study, we randomly picked two proteins, SOD2 and Sftpd, and checked their expression through IF and IHC, respectively. We found a significantly higher level of SOD2 expression in the infected 4 dpi tissues than 4 dpi mock-infected or 14 dpi-infected tissues (Figure 3A). Similarly, analysis of Sftpd expression showed lower expression of this protein in bronchial epithelial cells of 4 dpi and 14-dpi infected lung tissues than 4 dpi mock-infected samples (Figure 3B). Together, these data successfully validated the results of the mass spectrometry-based proteomics analysis.

4 | DISCUSSION

Multiple studies across the globe have demonstrated that the hamster model of SARS-CoV-2 infection mimics the milder form of COVID-19 in humans. Earlier study by using USA-WA1/2020 (NR-52281, BEI Resources) isolate showed that 5×10^4 TCID₅₀ dose of viral infection in hamsters lead to weight loss and full recovery by 14 days.³³ However, an infection dose of 5×10^5 TCID₅₀ dose induced severe weight loss and partial mortality.³³ Similarly, in a different study with an infection dose of 8×10^4 TCID₅₀ of BetaCoV/Hong Kong/VM20001061/2020 (GISAID# EPI_ISL_412028) virus, the investigators have reported a self-limiting model of SARS-CoV-2 with the manifestation of earlier lung tissue damage followed by recovery.³⁴ All these studies also corroborate the self-limiting nature of this model as reported by others.^{16,18,20} In the recent study, Mohandas et al have used an Indian SARS-CoV-2 isolate (NIV-2020-770) at different infection doses and noticed that $10^{5.5}$ TCID₅₀ and $10^{4.5}$ TCID₅₀ infection dose of the virus manifested a self-limiting disease with lung pathologies at the earlier days of infection.³⁵ Based on the aforementioned studies we picked a dose of 10^5 TCID₅₀ for the inoculation of hamsters with our isolate IND-ILS01/2020 (GenBank accession ID- MW559533.2). Similar to the earlier report, our analyses also showed a non-lethal and self-limiting model of SARS-CoV-2 infection in hamster. The histopathological and viral analysis of lung samples clearly showed that 4 dpi- and 14 dpi-infected animals represent acute and convalescent

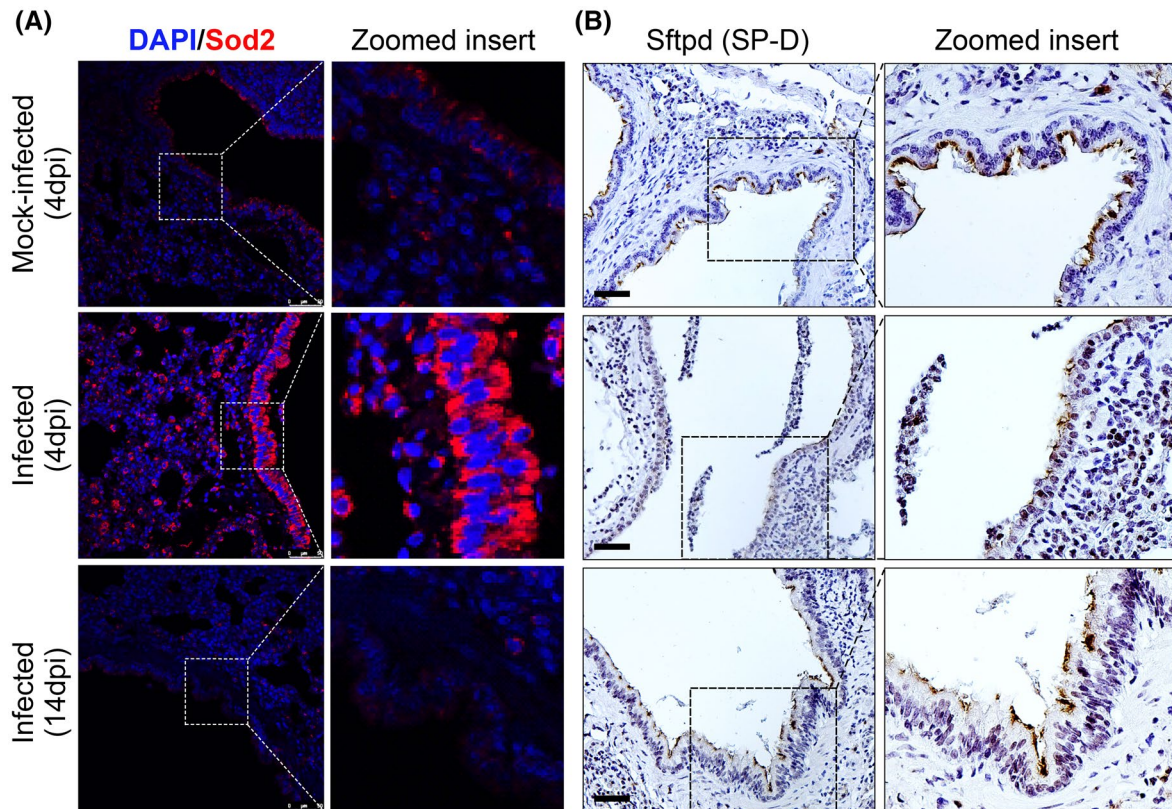


FIGURE 3 A, Immunofluorescence images of mock-infected or infected lung tissue sections showing the expression of Sod2 in bronchial and alveolar epithelial cells. B, Immunohistochemistry images of mock-infected or infected lung tissues showing expression of Sftpd in bronchial epithelial cells

stages of infection. The absence of the severe form of DAD features also corroborates earlier reports and indicates the limitation of this model.¹⁸

Our quantitative proteomic analysis data showed the dysregulation of biological processes such as “collagen fibril organization” and “actin cytoskeleton reorganization” in infected 4 dpi and “regulation of substrate adhesion-dependent cell spreading” and “endothelial cell migration” in the infected 14 dpi group. Collagen network organization occurs in response to tissue damage and is a part of the wound healing process and can trigger the onset of fibrosis. The actin cytoskeleton is an important cellular component, essential for maintaining the shape and structure of the cells. Many viruses promote the rearrangement of the host cell cytoskeleton to facilitate their dissemination.³⁶ We observed reduced expression of the proteins that contribute to dysregulation in actin polymerization at both 4 dpi and 14 dpi (Supplementary Tables S2 and S3). Reports also indicate that any alteration in the cell-matrix adhesion and extracellular matrix during injury repair can disrupt lung structure, further leading to lung damage. Our results also indicate the dysregulation of collagens in the 14 dpi lung tissues. The proteins associated with “endothelial cell migration” include Thymosin beta-4 (Tmsb4x) and High Mobility Group Box 1 (HMGB1), both of which have been reported to be potential therapeutic targets

in drug discovery. Tmsb4x is a small and water-soluble peptide known for its role in angiogenesis, wound healing, and increased metastatic potential of tumor cells.^{37,38} Its ability to induce fibrinolysis makes it an interesting molecular drug target. Recently, HMGB1 has also emerged as a potential target for therapeutic interventions for COVID-19. It is known to play a critical role in various infections, and its elevated expression has been reported in many viral infections, including COVID-19.^{39,40} This association further results in receptor-dependent responses suggesting its possible role in SARS-CoV-2 infection. Further studies are warranted to uncover the functional role of HMGB1 and evaluate its inhibitors in the COVID-19 treatment.

We also observed multiple pathways such as the dysregulation of complement and coagulation cascades, platelet degranulation, and ferroptosis upon viral infection across both the groups (4 dpi and 14 dpi). Existing literature also indicates the critical role of the complement pathway in pathogenesis and disease severity of SARS-CoV-2.^{41,42} The complement system serves as the host systems’ first response to foreign pathogens and regulates processes such as opsonization, chemotaxis, leukocyte recruitment, activation, and phagocytosis. However, unrestricted activation of this pathway contributes to acute and chronic inflammation, coagulation, cell injury, and facilitates multiple organ failure leading to death.⁴³

Significant dysregulation of complement and coagulation cascades along with elevated levels of D-dimer, fibrinogen, and von Willebrand factor have been observed in SARS-CoV-2-infected patients.⁴⁴ In the current study, we identified higher expression levels of C3, Fgb, Fga, Fgg, Serpinf2, and Cfb in 4 dpi hamster lung tissues as compared to mock-infected (4 dpi). The higher levels of these proteins were well studied as a marker of the activation of early complement and coagulation cascade. The significant enrichment of coagulation proteins in SARS-CoV-2-infected tissues indicates the disruption of coagulation mechanisms during SARS-CoV-2 infection. In addition, the higher expression of proteins such as Fgb, Fga, and Fgg identified in the study are also known to be involved in platelet activation. Platelets are non-nucleated cell fragments derived from megakaryocytes and essential for physiological hemostasis. Additionally, they are also known for their diverse role in inflammatory and immune response by acting as inflammatory effector cells.^{45,46} They also serve as an indispensable element in coagulation and inflammation and their activated state is associated with cancer progression.⁴⁷ Recently, the lung has also been proposed as a platelet biogenesis site, accounting for almost 50% of total platelets.⁴⁸ There are reports demonstrating the role of platelets in inflammatory lung syndromes/disorders such as acute respiratory distress syndrome (ARDS), chronic obstructive pulmonary disease (COPD), cystic fibrosis (CF), aspirin-exacerbated respiratory disease (AERD), and asthma.⁴⁶

Our pathway analysis with significantly downregulated proteins list also identified certain proteins involved in platelet activation (Col1a2, Gnaq, Rhoa), focal adhesion (Col1a2, Parva, Rhoa), and leukocyte transendothelial migration (Cldn18, Rhoa) in day 4 infected vs mock-infected animals. Even though the pathways are commonly shared among the up and downregulated proteins, the biological properties of each protein need to be considered while concluding.⁴⁹ The contrasting results from the pathway analysis of upregulated and downregulated proteins highlight the complex nature of these biological processes. Together, we believe that the current pathway analysis only gives a preliminary idea about the differentially expressed proteins in each group and their known biological function. Thus, more studies are required to elucidate the role of each pathway component in the pathophysiology of COVID-19.

Ferroptosis is a form of programmed cell death associated with unchecked lipid peroxidation due to the accumulation of lipid reactive oxygen species (ROS) in cells. Its role is well documented in pathophysiological processes of various diseases, such as tumors, nervous system diseases, ischemia-reperfusion injury, kidney injury, and blood diseases.⁵⁰ Iron is a pivotal component of the ferroptosis pathway and disruption of iron metabolism has been reported in COVID-19 patients.⁵¹ In our study, we observed increased ferritin (Fth1) levels in 4 dpi tissues sample. Its increased expression has also been reported in COVID-19 patients.^{52,53}

Studies on COVID-19 patients have demonstrated the usefulness of inflammatory markers such as procalcitonin, C-reactive protein, erythrocyte sedimentation rate, and serum amyloid A as an indicator of disease progression, however, little is known about the increased ferritin levels (hyperferritinemia) in these patients. In our study, we observed increased ferritin (Fth1) levels in both 4 dpi and 14 dpi lung tissues sample which corroborates with the recent findings where its increased expression has been reported in COVID-19 patients.^{52,53} Further studies are warranted to evaluate its role as a pathogenic mediator in COVID-19. In addition, we also report here increased levels of Fgb, and S100a10 in both groups when compared to mock-infected. Fgb is a blood-borne glycoprotein, with an active role in biological functions such as angiogenesis, wound healing, and inflammation.⁵⁴ It serves as a marker for vascular injuries along with other pathological conditions such as colitis, lung and kidney fibrosis.⁵⁵ Consistent with lung fibrosis observed in hamster post-infection with SARS-CoV-2 in the current study, Fgb was higher among both groups suggesting its role in blood clot formation where its higher expression is also reported in COVID-19 patients.⁵⁶ Calpactin I, belongs to the calcium-binding S100 family, and is ubiquitously expressed in the majority of cells. It is known for its role in wound healing, fibrinolysis, and angiogenesis.^{57,58} Binding of S100a10 with plasminogens facilitates its conversion to plasmin which in turn enhances the virulence and pathogenicity of SARS-CoV-2 by cleaving the spike protein.⁵⁹ Moreover, we identified lower levels of Srsf1 and Gnaq among both the infected group as compared to the mock-infected. Srsf1 belongs to the family of splicing regulators and its interaction with different proteins enables it to regulate a plethora of cellular pathways.⁶⁰ It plays a significant role in providing genomic stability and thus, viral infection results in the depletion of this protein along with other RNA binding proteins (RBPs) in the nucleus. Such association of the viral genome with host RBPs initiates apoptosis, further resulting in the release of viral particles during infection by compromising the host machinery.⁶¹ Gnaq, constitute the family of largest cell surface membrane receptors, expressed ubiquitously in mammalian cells, and known to be involved in multiple ways during viral infection.⁶² Studies have also demonstrated its role in regulating both innate and adaptive immunity.⁶³ Here we report the reduced expression of Gnaq in hamster lung tissues infected with SARS-CoV-2. Similar data were also observed in virus-infected macrophages implicating its role as a negative regulator of antiviral immune responses.⁶⁴

Pulmonary surfactant proteins constitute a type of lipoprotein complex comprising 90% lipids and 10% surfactant proteins (Sftpa, Sftpb, Sftpc, and Sftpd). These surfactant proteins contribute to providing defense against pathogens and play a critical role in efficient gaseous exchange at the air-liquid interface in the alveoli and provide lung stability.⁶⁵

We observed aberrant expression of the surfactant proteins (Sftpb, and Sftpd) across the 4 and 14 dpi-infected samples compared to the mock-infected samples suggesting the decline in the normal functionality of lung respiratory gaseous exchange owing to virus infection. The previous report has suggested the role of viral proteins in modulating the surfactant metabolism and thus, resulting in host immune compromise.⁶⁶

As reported earlier, we also noticed distinct damage to the epithelial-endothelial barrier in 4 dpi-infected lung tissues. This barrier system's damage is believed to be the major mediator of ARDS in different respiratory viral infections, including SARS-CoV-2.⁶⁷ The loss of the epithelial-endothelial barrier allows leakage of blood components into the alveolar lumen and lung interstitium. At the same time, it also allows the leakage of lung proteins into circulation.⁶⁸ In the recent past, it is shown that COVID-19 patients who developed ARDS have significantly higher IL-6 and Sftpd circulatory levels compared to patients who did not have ARDS.⁶⁹ These findings further indicate that the identification of pneumoproteins in circulation is an indicator of the severity of lung pathology. In our lung tissue proteome analysis, we noticed a significant downregulation of Sftpd protein in tissues with high lung pathology score (4 dpi), which suggests that certain proteins might have a differential pattern of expression level in circulation and at the primary site of infection (lungs). Based on several features of pulmonary surfactants, they are believed to have importance in COVID-19 pathogenesis, diagnosis or therapy. It has been proposed that a lower concentration of pulmonary surfactant is a critical risk factor for COVID-19.⁷⁰ Studies have also reported that concentrations of SP-A and SP-B were low in bronchoalveolar lavage (BAL) of patients before and after the onset of ARDS.⁷¹ The low level of pulmonary surfactant proteins detected in 4 dpi lung tissues underscores their possible role in the COVID-19 pathology. Altogether, these pulmonary lung surfactants might be considered as potential therapeutics to aid in COVID-19 treatment. Secretoglobin Family 1A Member 1 (Scgb1a1) encodes a member of the secretoglobulin family of small secreted proteins, a component of pulmonary surfactant, which is expressed in mucus-secreting cells. This protein is known for its anti-inflammatory/ immunomodulatory and anti-fibrotic functions.⁷² We identified severe downregulation of Scgb1a1 in the lung tissue post-infection (4 dpi), suggesting respiratory distress owing to virus-mediated lung injury. Some literature have also reported its altered expression following lung injury and where its absence is marked with the greater inflammatory response.⁷³⁻⁷⁵ It is also known to regulate alveolar macrophage-mediated inflammatory response upon virus invasion.⁷⁵ However, further studies are required to study its effectiveness and the underlying mechanism(s) associated with virus infection. Further, it suggests the usefulness of the

hamster model of SARS-CoV-2 infection in evaluating the therapeutic efficacies of these proteins for COVID-19.

Through an ultra-high-throughput clinical proteomics approach, Messner et al, identified protein expression signatures in serum/plasma samples including complement factors, components of coagulation systems, immunomodulators, and proinflammatory factors that can classify COVID-19 patients based on WHO grading.⁴ The authors have proposed 27 protein groups (23 upregulated and 4 downregulated) as potential biomarkers of disease severity. Out of these upregulated proteins, we noticed six proteins Complement factor B (Cfb), Fibrinogens (Fga, Fgb, Fgg), Haptoglobin (Hp), and Galectin-3-binding protein (Lgals3bp) are also present in the list of upregulated proteins at 4 dpi vs mock-infected groups of our study. However, albumin (Alb), and transferrin (Tf) whose downregulation correlated with COVID-19 severity⁴ are found to be upregulated at the 4 dpi infection group of our study. There are multiple possibilities for this discrepancy like (a) blood proteome and lung proteome might be different in SARS-CoV-2-infected humans or animals, (b) difference in techniques or methods used to analyze samples, and (c) species-dependent differential (hamsters or human) host response to SARS-CoV-2 infection. Similarly, proteomic and metabolomic profiling of serum samples obtained from 46 COVID-19 and 53 control individuals showed deregulation of three major pathways namely complement system, macrophage function, and platelet degranulation in severe COVID-19 patients.⁴¹ A study by Park et al, employed an in-depth proteome profiling of undepleted plasma revealed signatures of proteins involved in neutrophil activation, platelet function, and T cell suppression.⁶ Based on their findings, the authors have proposed specific plasma proteins as predictive biomarkers of COVID-19.⁶ In a different study, proteomic analysis of serum samples from early COVID-19 patients also identified differentially expressed proteins known to have a function in SARS-CoV-2 infection-associated inflammation and immune signaling.⁷ The findings of our study also corroborate the aforementioned findings.

Efforts to investigate the alteration in bronchoalveolar lavage fluid (BALF) proteome in COVID-19 patients compared to the non-COVID-19 controls demonstrated that SARS-CoV-2 infection induces alteration in BALF proteome with enrichment of proteins involved in proinflammatory cytokine-mediated signaling and oxidative stress response.⁵ Superoxide dismutase (SOD) is vital for human health and upregulation of SOD2 expression upon challenge with human pathogens suggests its role in immune response. Antioxidant enzymes such as SOD2 are pivotal to protect from free superoxide anion, which can damage epithelial cells and impair their function. Thus, enhanced expression of Sod2 in SARS-CoV-2-infected hamster lungs, suggests the upregulation of antioxidant response

to prevent oxidative stress-induced tissue damage, lung injury, and respiratory distress.

Taken together, the current study highlights the proteomic alterations caused owing to SARS-CoV-2 infection during the course of infection and provides an insight on the molecular pathogenesis and possible therapeutic targets of COVID-19. Importantly, the current study provides strong molecular evidence that shows the similarities between SARS-CoV-2 infection in humans and hamsters and supports the clinical relevance of this model in COVID-19 research. However, the present study has some limitations of the small sample size considered for the analysis and use of limited experimental conditions (single viral dose and strain). This demands similar extensive research in a large number of animals and different experimental conditions for further validation. Moreover, due to the small number of animals, the effects of age, sex, and comorbidities await further investigation. The unavailability of complete genome information of Syrian golden hamsters has also substantially restricted our findings. We hope in the future with the availability of complete genome sequence and hamster-specific reagents like antibodies will help in obtaining more relevant information from our current findings.

ACKNOWLEDGMENTS

The study is financially supported by the DBT-Institute of Life Science (ILS) and DBT-BIRAC (BT/CS0004/CS/02/20). We sincerely acknowledge the technical supports given by Madan Mohan Mallick, Sushanta Kumar Swain, and Bhabani S. Sahoo, ILS. We are thankful to Dr. Kunal Sahu, Veterinary pathologist, ILS for his valuable support in the histopathological analysis. We are grateful to Dr. Taruna Madan Gupta, NIRRH, Mumbai, for providing us the Sftpd (SP-D) antibody. Voddu Suresh is a recipient of the Council of Scientific and Industrial Research (CSIR) students' research fellowship, Government of India. Varshasnata Mohanty is a recipient of the Women Scientist-A award from the Department of Science and Technology (DST), Government of India. G. H. Syed acknowledges the support from DBT-Wellcome Trust India Alliance (IA/I/15/1/501826).

CONFLICT OF INTEREST

The authors declare that the research was conducted in the absence of any commercial or financial relationships that could be construed as a potential conflict of interest.

AUTHOR CONTRIBUTIONS

S. Senapati and G. H. Syed, conceived the idea, and supervised the overall experiments. V. Suresh, and K. Avula contributed to animal inoculation and tissue analysis. B. Singh, K. Avula, and G. H. Syed contributed to viral copy number estimation and

viral culture. V. Mohanty and R. K. Reddy carried out sample preparation for proteomics analysis. V. Mohanty, A. Ghosh, and V. Suresh were involved in proteomics data analysis, data interpretation, prepared figures and tables. A. R. Suryawanshi and S. K. Raghav crosschecked the bioinformatics data analysis. V. Suresh and D. Parida did tissue processing and staining. S. Senapati carried out the pathological evaluation of tissue sections as one of the evaluators. S. Chattopadhyay, P. Prasad, R. K. Swain, R. Dash, and A. Parida facilitated in establishing Standard Operating Procedures (SOPs) for ABSL3-related activities and intellectually contributed in manuscript writing and interpretation of the data. All authors were involved in manuscript writing and editing.

DATA AVAILABILITY STATEMENT

The raw data files and the MSF files were submitted to the PRIDE partner repository⁷⁶ with data set identifier PXD024547.

ORCID

Gulam Hussain Syed  <https://orcid.org/0000-0001-8540-6162>

Shantibhusan Senapati  <https://orcid.org/0000-0001-7108-8255>

REFERENCES

1. Sinha P, Matthay MA, Calfee CS. Is a "Cytokine Storm" relevant to COVID-19? *JAMA Intern Med.* 2020;180:1152-1154.
2. Ackermann M, Verleden SE, Kuehnel M, et al. Pulmonary vascular endothelialitis, thrombosis, and angiogenesis in COVID-19. *N Engl J Med.* 2020;383:120-128.
3. McGonagle D, O'Donnell JS, Sharif K, Emery P, Bridgewood C. Immune mechanisms of pulmonary intravascular coagulopathy in COVID-19 pneumonia. *Lancet Rheumatol.* 2020;2:e437-e445.
4. Messner CB, Demichev V, Wendisch D, et al. Ultra-high-throughput clinical proteomics reveals classifiers of COVID-19 infection. *Cell Systems.* 2020;11(11-24):e14.
5. Zeng HL, Chen D, Yan J, et al. Proteomic characteristics of bronchoalveolar lavage fluid in critical COVID-19 patients. *FEBS J.* 2020. <https://doi.org/10.1111/febs.15609>
6. Park J, Kim H, Kim SY, et al. In-depth blood proteome profiling analysis revealed distinct functional characteristics of plasma proteins between severe and non-severe COVID-19 patients. *Sci Rep.* 2020;10:22418.
7. Hou X, Zhang X, Wu X, et al. Serum protein profiling reveals a landscape of inflammation and immune signaling in early-stage COVID-19 infection. *Mol Cell Proteomics.* 2020;19:1749-1759.
8. Akgun E, Tuzuner MB, Sahin B, et al. Altered molecular pathways observed in naso-oropharyngeal samples of SARS-CoV-2 patients. *medRxiv.* 2020;2005:2014.20102558
9. Leng L, Cao R, Ma J, et al. Pathological features of COVID-19-associated lung injury: a preliminary proteomics report based on clinical samples. *Signal Transduct Target Ther.* 2020;5:240.
10. Wu M, Chen Y, Xia H, et al. Transcriptional and proteomic insights into the host response in fatal COVID-19 cases. *Proc Natl Acad Sci USA.* 2020;117:28336-28343.

11. Nie X, Qian L, Sun R, et al. Multi-organ proteomic landscape of COVID-19 autopsies. *Cell*. 2021;184(775-791):e714.
12. Bradley BT, Maioli H, Johnston R, et al. Histopathology and ultrastructural findings of fatal COVID-19 infections in Washington State: a case series. *Lancet*. 2020;396:320-332.
13. Grasselli G, Tonetti T, Protti A, et al. Pathophysiology of COVID-19-associated acute respiratory distress syndrome: a multicentre prospective observational study. *Lancet. Respir Med*. 2020;8:1201-1208.
14. Munoz-Fontela C, Dowling WE, Funnell SGP, et al. Animal models for COVID-19. *Nature*. 2020;586:509-515.
15. Ehaideb SN, Abdullah ML, Abuyassin B, Bouchama A. Evidence of a wide gap between COVID-19 in humans and animal models: a systematic review. *Crit Care*. 2020;24:594.
16. Imai M, Iwatsuki-Horimoto K, Hatta M, et al. Syrian hamsters as a small animal model for SARS-CoV-2 infection and countermeasure development. *Proc Natl Acad Sci USA*. 2020;117:16587-16595.
17. Lee AC, Zhang AJ, Chan JF, et al. Oral SARS-CoV-2 inoculation establishes subclinical respiratory infection with virus shedding in golden syrian hamsters. *Cell Rep. Med*. 2020;1:100121.
18. Rosenke K, Meade-White K, Letko M, et al. Defining the Syrian hamster as a highly susceptible preclinical model for SARS-CoV-2 infection. *Emerg Microbes Infect*. 2020;9:2673-2684.
19. Chan JF, Yuan S, Zhang AJ, et al. Surgical mask partition reduces the risk of noncontact transmission in a golden Syrian hamster model for coronavirus disease 2019 (COVID-19). *Clin Infect Dis*. 2020;71:2139-2149.
20. Chan JF, Zhang AJ, Yuan S, et al. Simulation of the clinical and pathological manifestations of coronavirus disease 2019 (COVID-19) in a golden Syrian hamster model: implications for disease pathogenesis and transmissibility. *Clin Infect Dis*. 2020;71:2428-2446.
21. Lee CY, Lowen AC. Animal models for SARS-CoV-2. *Curr Opin Virol*. 2021;48:73-81.
22. Suresh V, Parida D, Minz AP, Sethi M, Sahoo BS, Senapati S. Tissue distribution of ACE2 protein in Syrian golden hamster (*Mesocricetus auratus*) and its possible implications in SARS-CoV-2 related studies. *Front Pharmacol*. 2020;11:579330.
23. Li C, Chen YX, Liu FF, et al. Absence of vaccine-enhanced disease with unexpected positive protection against SARS-CoV-2 by inactivated vaccine given within three days of virus challenge in Syrian hamster model. *Clin Infect Dis*. 2021. <https://doi.org/10.1093/cid/ciab083>
24. Suresh V, Sundaram R, Dash P, et al. Macrophage migration inhibitory factor of Syrian golden hamster shares structural and functional similarity with human counterpart and promotes pancreatic cancer. *Sci Rep*. 2019;9:15507.
25. Kale K, Vishwekar P, Balsarkar G, Jassawalla MJ, Sawant G, Madan T. Differential levels of surfactant protein A, surfactant protein D, and progesterone to estradiol ratio in maternal serum before and after the onset of severe early-onset preeclampsia. *Am J Reprod Immunol*. 2020;83:e13208.
26. Kim SJ, Syed GH, Siddiqui A. Hepatitis C virus induces the mitochondrial translocation of Parkin and subsequent mitophagy. *PLoS Pathog*. 2013;9:e1003285.
27. Gordon DE, Jang GM, Bouhaddou M, et al. A SARS-CoV-2 protein interaction map reveals targets for drug repurposing. *Nature*. 2020;583:459-468.
28. Thompson A, Schäfer J, Kuhn K, et al. Tandem mass tags: a novel quantification strategy for comparative analysis of complex protein mixtures by MS/MS. *Anal Chem*. 2003;75:1895-1904.
29. Kim MS, Pinto SM, Getnet D, et al. A draft map of the human proteome. *Nature*. 2014;509:575-581.
30. Kuleshov MV, Jones MR, Rouillard AD, et al. Enrichr: a comprehensive gene set enrichment analysis web server 2016 update. *Nucleic Acids Res*. 2016;44:W90-W97.
31. Leist SR, Dinnon KH 3rd, Schafer A, et al. A mouse-adapted SARS-CoV-2 induces acute lung injury and mortality in standard laboratory mice. *Cell*. 2020;183(1070-1085):e1012.
32. Mi H, Ebert D, Muruganujan A, et al. PANTHER version 16: a revised family classification, tree-based classification tool, enhancer regions and extensive API. *Nucleic Acids Res*. 2021;49:D394-D403.
33. Tostanoski LH, Wegmann F, Martinot AJ, et al. Ad26 vaccine protects against SARS-CoV-2 severe clinical disease in hamsters. *Nat Med*. 2020;26:1694-1700.
34. Sia SF, Yan LM, Chin AWH, et al. Pathogenesis and transmission of SARS-CoV-2 in golden hamsters. *Nature*. 2020;583:834-838.
35. Mohandas S, Yadav PD, Shete-Aich A, et al. Immunogenicity and protective efficacy of BBV152, whole virion inactivated SARS-CoV-2 vaccine candidates in the Syrian hamster model. *iScience*. 2021;24:102054.
36. Tresoldi I, Sangiuolo CF, Manzari V, Modesti A. SARS-COV-2 and infectivity: possible increase in infectivity associated to integrin motif expression. *J Med Virol*. 2020;92:1741-1742.
37. Goldstein AL, Hannappel E, Sosne G, Kleinman HK. Thymosin β 4: a multi-functional regenerative peptide. Basic properties and clinical applications. *Expert Opin Biol Ther*. 2012;12:37-51.
38. Goldstein AL, Kleinman HK. Advances in the basic and clinical applications of thymosin β 4. *Expert Opin Biol Ther*. 2015;15(Suppl 1):S139-S145.
39. Kang R, Chen R, Zhang Q, et al. HMGB1 in health and disease. *Mol Aspects Med*. 2014;40:1-116.
40. Chen R, Huang Y, Quan J, et al. HMGB1 as a potential biomarker and therapeutic target for severe COVID-19. *Heliyon*. 2020;6:e05672.
41. Shen B, Yi X, Sun Y, et al. Proteomic and metabolomic characterization of COVID-19 patient sera. *Cell*. 2020;182(59-72):e15.
42. Li Y, Wang Y, Liu H, et al. Urine proteome of COVID-19 patients. *Urine (Amst)*. 2020;2:1-8.
43. Noris M, Remuzzi G. Overview of complement activation and regulation. *Semin Nephrol*. 2013;33:479-492.
44. Vinayagam S, Sattu K. SARS-CoV-2 and coagulation disorders in different organs. *Life Sci*. 2020;260:118431.
45. Gomez-Casado C, Villaseñor A, Rodriguez-Nogales A, Bueno JL, Barber D, Escribese MM. Understanding platelets in infectious and allergic lung diseases. *Int J Mol Sci*. 2019;20:1730.
46. Middleton EA, Weyrich AS, Zimmerman GA. Platelets in pulmonary immune responses and inflammatory lung diseases. *Physiol Rev*. 2016;96:1211-1259.
47. Ji Y, Sheng L, Du X, Qiu G, Su D. Elevated platelet count is a strong predictor of poor prognosis in stage I non-small cell lung cancer patients. *Platelets*. 2015;26:138-142.
48. Lefrancais E, Ortiz-Munoz G, Caudrillier A, et al. The lung is a site of platelet biogenesis and a reservoir for haematopoietic progenitors. *Nature*. 2017;544:105-109.
49. Hong G, Zhang W, Li H, Shen X, Guo Z. Separate enrichment analysis of pathways for up- and downregulated genes. *J R Soc Interface*. 2014;11:20130950.
50. Li J, Cao F, Yin HL, et al. Ferroptosis: past, present and future. *Cell Death Dis*. 2020;11:88.

51. Edeas M, Saleh J, Peyssonnaux C. Iron: Innocent bystander or vicious culprit in COVID-19 pathogenesis? *Int J Infect Dis.* 2020;97:303-305.
52. Vargas-Vargas M, Cortes-Rojo C. Ferritin levels and COVID-19. *Rev Panam Salud Publica.* 2020;44:e72.
53. Fox SE, Akmatbekov A, Harbert JL, Li G, Quincy Brown J, Vander Heide RS. Pulmonary and cardiac pathology in African American patients with COVID-19: an autopsy series from New Orleans. *Lancet Respir Med.* 2020;8:681-686.
54. Weisel JW, Litvinov RI. Fibrin formation, structure and properties. *Subcell Biochem.* 2017;82:405-456.
55. Davalos D, Akassoglou K. Fibrinogen as a key regulator of inflammation in disease. *Semin Immunopathol.* 2012;34:43-62.
56. Helms J, Tacquard C, Severac F, et al. High risk of thrombosis in patients with severe SARS-CoV-2 infection: a multicenter prospective cohort study. *Intensive Care Med.* 2020;46:1089-1098.
57. Surette AP, Madureira PA, Phipps KD, Miller VA, Svenningsson P, Waisman DM. Regulation of fibrinolysis by S100A10 in vivo. *Blood.* 2011;118:3172-3181.
58. Madureira PA, Surette AP, Phipps KD, Taboski MA, Miller VA, Waisman DM. The role of the annexin A2 heterotetramer in vascular fibrinolysis. *Blood.* 2011;118:4789-4797.
59. Ji HL, Zhao R, Matalon S, Matthay MA. Elevated Plasmin(ogen) as a common risk factor for COVID-19 susceptibility. *Physiol Rev.* 2020;100:1065-1075.
60. Das S, Krainer AR. Emerging functions of SRSF1, splicing factor and oncoprotein, in RNA metabolism and cancer. *Mol Cancer Res.* 2014;12:1195-1204.
61. Rogan PK, Mucaki EJ, Shirley BC. A proposed molecular mechanism for pathogenesis of severe RNA-viral pulmonary infections. *F1000Res.* 2020;9:943.
62. Sodhi A, Montaner S, Gutkind JS. Viral hijacking of G-protein-coupled-receptor signalling networks. *Nat Rev Mol Cell Biol.* 2004;5:998-1012.
63. Wang Y, Li Y, Shi G. The regulating function of heterotrimeric G proteins in the immune system. *Arch Immunol Ther Exp (Warsz).* 2013;61:309-319.
64. Wang N, Huang H, Xiong Q, et al. GNAQ negatively regulates antiviral innate immune responses in a calcineurin-dependent manner. *J Immunol.* 2019;203:1288-1297.
65. Glasser JR, Mallampalli RK. Surfactant and its role in the pathobiology of pulmonary infection. *Microbes Infect.* 2012;14:17-25.
66. Islam A, Khan MA. Lung transcriptome of a COVID-19 patient and systems biology predictions suggest impaired surfactant production which may be druggable by surfactant therapy. *Sci Rep.* 2020;10:19395.
67. Short KR, Kroeze E, Fouchier RAM, Kuiken T. Pathogenesis of influenza-induced acute respiratory distress syndrome. *Lancet Infect Dis.* 2014;14:57-69.
68. Doyle IR, Bersten AD, Nicholas TE. Surfactant proteins-A and -B are elevated in plasma of patients with acute respiratory failure. *Am J Respir Crit Care Med.* 1997;156:1217-1229.
69. Kerget B, Kerget F, Koçak AO, et al. Are serum interleukin 6 and surfactant protein D levels associated with the clinical course of COVID-19? *Lung.* 2020;198:777-784.
70. Weiskirchen R. Severity of coronavirus disease 2019 (COVID-19): does surfactant matter? *Front Microbiol.* 2020;11:1905.
71. Greene KE, Wright JR, Steinberg KP, et al. Serial changes in surfactant-associated proteins in lung and serum before and after onset of ARDS. *Am J Respir Crit Care Med.* 1999;160:1843-1850.
72. Mukherjee AB, Zhang Z, Chilton BS. Uteroglobin: a steroid-inducible immunomodulatory protein that founded the Secretoglobin superfamily. *Endocr Rev.* 2007;28:707-725.
73. Matsumoto T, Fujita M, Hirano R, et al. Chronic *Pseudomonas aeruginosa* infection-induced chronic bronchitis and emphysematous changes in CCSP-deficient mice. *Int J Chron Obstruct Pulmon Dis.* 2016;11:2321-2327.
74. Wang SZ, Rosenberger CL, Bao YX, Stark JM, Harrod KS. Clara cell secretory protein modulates lung inflammatory and immune responses to respiratory syncytial virus infection. *J Immunol (Baltimore, Md: 1950).* 2003;171:1051-1060.
75. Xu M, Yang W, Wang X, Nayak DK. Lung secretoglobin Scgb1a1 influences alveolar macrophage-mediated inflammation and immunity. *Front Immunol.* 2020;11:584310.
76. Hermjakob H, Apweiler R. The proteomics identifications database (PRIDE) and the ProteomeExchange Consortium: making proteomics data accessible. *Expert Rev Proteomics.* 2006;3:1-3.

SUPPORTING INFORMATION

Additional Supporting Information may be found online in the Supporting Information section.

How to cite this article: Suresh V, Mohanty V, Avula K, et al. Quantitative proteomics of hamster lung tissues infected with SARS-CoV-2 reveal host factors having implication in the disease pathogenesis and severity. *The FASEB Journal.* 2021;35:e21713.
<https://doi.org/10.1096/fj.202100431R>